Germanium Surface Wet-Etch-Reconditioning for Porous Lift-off and Substrate Reuse

Alexandre Chapotot, Bouraoui Ilahi, Javier Arias-Zapata, Tadeáš Hanuš, Ahmed Ayari, Gwenaëlle Hamon, Jinyoun Cho, Kristof Dessein, Maxime Darnon, Abderraouf Boucherif

Manuscript Revised

Germanium Surface Wet-Etch-Reconditioning for Porous Lift-off and Substrate Reuse

Alexandre Chapotot[1,2,], Bouraoui Ilahi[1,2], Javier Arias-Zapata[1,2], Tadeáš Hanuš [1,2], Ahmed Ayari[1,2], Gwenaëlle Hamon[1,2], Jinyoun Cho[3], Kristof Dessein[3], Maxime Darnon[1,2], Abderraouf Boucherif[1,2,*]*

[1]Institut Interdisciplinaire d′Innovation Technologique (3IT), Université de Sherbrooke, 3000 Boulevard Université, Sherbrooke, J1K 0A5 Québec, Canada
[2]Laboratoire Nanotechnologies Nanosystèmes (LN2) - CNRS IRL-3463, Institut Interdisciplinaire d′Innovation Technologique (3IT), Université de Sherbrooke, 3000 Boulevard Université, Sherbrooke, J1K 0A5 Québec, Canada
[3] Umicore Electro-Optic Materials, Watertorenstraat 33, 2250, Olen, Belgium

Corresponding authors : alexandre.chapotot@usherbrooke.ca (A. Chapotot) ; Abderraouf.boucherif@usherbrooke.ca (A. Boucherif).

KEYWORDS: Germanium, Wet etching, Porous Germanium, Polishing, Substrate Reuse, Porous Lift-off.

ABSTRACT

Reducing both the cost and weight of Germanium (Ge)-based devices is a key concern in extending these technologies to mainstream applications. In this framework, the porous Ge lift-off, based on a mesoporous Ge layer (PGe), shaped by bipolar electrochemical etching (BEE), constitutes an appealing strategy allowing the separation of lightweight, flexible, and low-cost devices and substrate reuse. However, after the device detachment, the broken pillar residues on the host substrate's surface prevent its reuse. Here, we report on the development and application of a reconditioning process based on an aqueous $HF:H_2O_2:H_2O$ (10:80:10, v-v-v) mixture without the need for Chemical Mechanical Polishing (CMP). We found that a mixed kinetic- and diffusion-controlled wet etching leads to surface polishing. Flat reconditioned substrates with

low surface roughness (<2.5 nm RMS) are successfully obtained from detached surfaces with various pillar sizes up to 500 nm in diameter. The substrate reusability is demonstrated by achieving a new porous layer on a reconditioned substrate with an RMS roughness of 2.2 nm, ready for a second round of the membrane's epitaxial growth. These results demonstrate a CMP-free, reliable Ge substrate reconditioning process, paving the way towards substrate multi-reuse and consequent devices' weight and cost reduction.

1. INTRODUCTION

Germanium (Ge) is a material of choice for the design of various devices such as batteries and biosensors [1,2]. However, it is mostly used as a platform for III-V materials integration for high-power-density optoelectronic and photovoltaic (PV) devices [3–5]. Substrates of this rare and critical material represent approximately 30-40% of the overall device cost, preventing its large-scale adoption for mainstream terrestrial PV applications [6,7]. Although standard 100 mm Ge wafers have a thickness of around 175 µm, the absorber thickness is much thinner (~2-5 µm), resulting in a substantial part of the Ge substrate being used only as a mechanical support for manufacturing [8]. This substrate thickness results in a significant cell weight, which is another challenging factor, especially for space PV applications [8], and may require being thinned down [9]. Furthermore, wasting Ge material is undesirable from an environmental perspective [10]. These technological, economic, and sustainable considerations are calling for the development of a process flow that reduces the consumption of Ge, while targeting lightweight and low-cost devices.

Recently, thin Ge film release technologies have been developed, opening the way to substrate reuse, which constitutes a stepping-stone towards reducing both the device's weight and cost. Accordingly, several methods have been reported, namely Epitaxial Lift-Off (ELO) [11],

spalling [12], Germanium-On-Nothing (GON) [13,14], Smart Cut technology [15], patterned graphene [16,17], and porosification lift-off [18]. Among these technologies, the porous approaches, with either dry [13,14] or wet methods [19], have gained recent momentum. Indeed, the electrochemical porous Ge (PGe) has focused recent attention on pore formation mechanisms [20–23] and already demonstrated both good epitaxial layer quality for Ge and III-V layers [24–26] as well as good solar cell performances [27]. However, after the detachment, the roughness of the mother substrate is too high for direct reuse due to the presence of broken pillars and nanostructure remnants. Therefore, it is necessary to recondition the substrate. Up to date, substrate reconditioning and reuse after the lift-off process have not been concretely considered outside the promises of the conventional chemical and mechanical polishing (CMP) approach [7]. Although the efficiency of the CMP technique is widely recognized, it introduces additional processing costs (between $9 to $38 per polishing [6,7]). Therefore, the development of a cost-effective and affordable route for Ge substrate reconditioning remains a key challenge.

Based on a similar strategy developed for silicon (Si) substrate reconditioning [28], wet etching is a potential reconditioning method of Ge substrates without CMP use. This approach relies on the oxidation of surface Ge atoms by an oxidizing agent, and the formation of soluble complexes by a complexing agent [29,30]. Nitric Acid (HNO_3)-based solutions, in which nitric acid acts as a Ge oxidizing agent, have high etch rates of 10-100 µm/min due to an electrochemical reaction between nitric acid and Ge [9,31,32]. This electrochemical reaction provides the formation of nitrous acid during the reduction of HNO_3, allowing the production of highly oxidative N(III) species [31]. These solutions are well suited for substrate thinning [9]. However, for applications in reconditioning, low etch rates are generally preferred to limit excessive loss of the material during the surface flattening. This can be achieved by the use of hydrogen peroxide (H_2O_2)-

based solutions, which allows lower etch rates [31]. H_2O_2-systems are based on a purely chemical mechanism in which $[Ge(OH)_2]^{2+}$ is a surface intermediate formed through surface Ge oxides [29,33,34]. This results in etching rates around 1 μm/min. By using low etch rates, the thickness of Ge dissolved during the reconditioning process can be limited, while allowing a reasonable process time compatible with industrial standards. In addition, complexing agents can be added to the oxidizing agent to increase the etch rate of the oxidized surface such as NH_4OH in dilute Ammonia Peroxide Mixture (APM, NH_4OH:H_2O_2:H_2O, 1:1:5, v-v-v), HCl in dilute Hydrochloric acid Peroxide Mixture (HPM, HCl:H_2O_2:H_2O, 1:1:7, v-v-v), or HF in HF-based solutions (HF:H_2O_2:H_2O, 1:3:6, v-v-v) which are routinely used in Ge surface cleaning processes [9,30,35].

In our previous study [26], we focused on presenting the proof of concept for the Porous germanium Efficient Epitaxial LayEr Release (PEELER) process, offering an overview of all stages, ranging from porosification and membrane growth to detachment and substrate reconditioning. In the current work, we report the detailed reconditioning process applied to a different PGe structure with a widely tunable thermally induced reorganization process. These new findings expand the scope of the proposed reconditioning method to encompass microscale-sized pillars. Additionally, we offer a comprehensive and in-depth analysis of the effects of etching mixtures comprising HF and H_2O_2 solutions on the porous nanostructures, highlighting its potential as a universal reconditioning technique for various pillar shapes and densities. Indeed, the APM, HPM, and HF-based mixtures are investigated in the framework of the substrate reconditioning after porous lift-off, allowing reusing the reconditioned substrate for a second PEELER cycle. Our work represents the foundational step for an easily accessible, cost-effective, and scalable Ge wet etch reconditioning and reuse process.

2. METHODS

2.1. Ge samples and solutions:

P-type gallium-doped, 100 mm Ge wafers with resistivity 7-30 mΩ·cm and (100) crystal orientation with 6° miscut towards (111), as well as hydrofluoric acid (HF, 49 wt.%), hydrogen peroxide (H_2O_2, 30 wt.%), hydrochloric acid (HCl, 37 wt.%), ammonia solution (NH_4OH, 20-30 wt.%), ultrapure water (H_2O), and ethanol (EtOH, 99 wt.%) are used in this study.

2.2. Porous lift-off process:

The porous lift-off process flow used in this study is based on the PEELER process reported in our previous work [26] and is described in Fig. 1 (a). ***(i)*** A PGe layer is shaped by electrochemical etching on top of a Ge wafer (Fig. 1 (b)). ***(ii)*** After porosification, the Ge membrane (NM) is grown on top of the porous structure with a two-step growth. The thermal budget during epitaxy leads to the reorganization of the PGe layer into pillars separated by voids. A typical cross-sectional scanning electron microscope (SEM) image of the obtained structure after epitaxy is shown in Fig. 1 (c). The epitaxial Ge layer exhibits a single crystal quality (Fig. S1) with low surface roughness (< 1 nm RMS, Fig. S1). ***(iii)*** Finally, the crystalline Ge NM is separated from the substrate by means of the voided-separation layer, using normal mechanical pulling. During this separation method, the stress accumulation due to the mechanical pulling will initiate cracks in the pillars, allowing the NM release [36,37]. Consequently, as shown in Fig. 1 (d), the NM detachment leaves broken pillar residues on the detached surface of the mother substrate, leading to a high RMS roughness above 20 nm, measured by atomic force microscopy (AFM) presented in the inset of Fig. 1 (d).

2.3. Ge porosification:

PGe layers are shaped by bipolar electrochemical etching (BEE) using HF:EtOH (4:1, v-v) electrolyte in a custom-made cell with a Cu working electrode and Pt counter-electrode following a previously developed process [20,21]. The Ge wafer is cleaned in HF for 5 min followed by a 5 min EtOH rinse and dried under N_2 flux before porosification. A homogeneous 220 nm-thick, PGe layer (Fig. 1 (b)) with a porosity of around 52% and a sponge-like morphology is formed over the full wafer using 1 $mA \cdot cm^{-2}$ symmetric etching/passivation current densities with 1 s etching/passivation pulse duration. Further details on PGe formation and properties can be found elsewhere [21].

2.4.Ge epitaxial growth:

After porosification, the wafer is rinsed in EtOH, dried under N_2 flux, and immediately introduced into the epitaxy reactor for Ge epitaxy. The Ge NMs are grown by a two-step process with a 200 nm-thick low-temperature Ge buffer layer deposited at 300 °C followed by a high-temperature growth at 450 °C, in a hybrid VG Semicon V90F CBE/MBE reactor. The epitaxial growths are performed under high vacuum (~10^{-6} Torr) with a solid Ge source with K-cell heated to 1250 °C; the growth rate was 0.5 µm/h.

2.5.Thermal annealing:

After epitaxial growth, similar as-grown structures are subjected to post-growth thermal treatments at 600 °C and 700 °C for 1 h under forming gas. These thermal treatments are carried out using a tubular furnace (Carbolite Gero Limited, UK). After NM's detachment, the pillar's diameter has been measured with image processing software ImageJ on various 10x10 µm probed surfaces with SEM top-view scans.

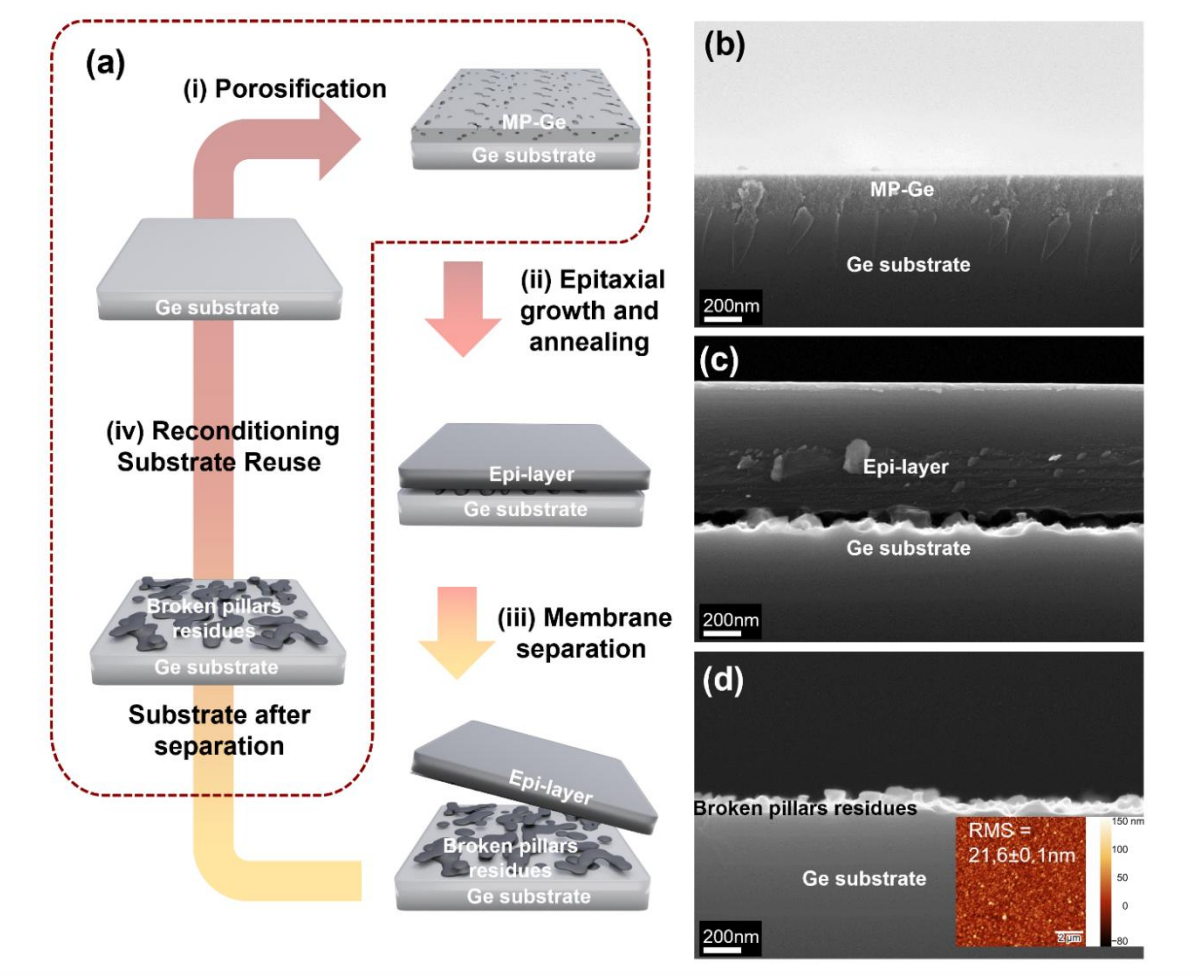

Fig. 1: (a) Process-flow of the porous lift-off approach. (b) SEM cross-sectional image of a porous layer. (c) SEM cross-sectional image after the epitaxial growth. (d) SEM cross-sectional image of the Ge substrate after NM separation, with a typical AFM scan as inset.

2.6.Ge surface wet etching:

Wet etching experiments are conducted at room temperature with a rotation rate of 600 RPM. The etch rates are determined by a lithographic process of patterned stripes and profilometer measurements before and after the wet etching on bulk Ge wafers. Since the targeted substrates to be reconditioned have nanostructured surfaces with only tens of nm average height, and considering the µm-scale etched depth, the obtained etch rate on PGe samples is considered the same as those determined for the bulk Ge wafer. All ratios shown in

this study are volume ratios (v-v-v). Based on the determined etch rate, we selected the etching time to achieve a 5 µm thickness removal of Ge. The etching depth has been verified using profilometer measurements.

2.7. Material characterizations:

Cross-section and top-view images are obtained using scanning electron microscopy (LEO 1540 XB ®) with an acceleration voltage of 5 and 20 keV and a working distance between 4 and 5 nm. The surface roughness is measured by atomic force microscopy (AFM) with a Veeco Dimension 3000 in tapping mode, with a scan size of 5 × 5 μm^2 for porous structures and 10 × 10 μm^2 for etched structures, both with a resolution of 512 x 512 pixels. Each sample is scanned on three different areas, allowing determining the mean RMS roughness values and their standard deviation. A Dektak 150 from Veeco (Bruker) is used to determine the solution etch rates by a profilometer measurement. Electrochemical etching is performed and monitored with SP-50 from Biologic that enables current-voltage measurement in real-time. The crystalline quality of the Ge epi-layer is evaluated by X-ray diffractometer (SMARTLAB, Rigaku). Finally, the critical angles of the PGe layer and the substrate are determined by X-ray reflectometry (SMARTLAB, Rigaku) and used to calculate the porosity of the porous layer as follows (Eq. 1)[21,38].

$$p\ (\%) = \left(1 - \left(\frac{\theta_{PGe}}{\theta_{Ge}}\right)^2\right) \times\ 100\ \#(\mathbf{1})$$

With θ_{PGe} the critical angle of the PGe layer and θ_{Ge} the substrate critical angle (0.59 ° for Ge).

3. RESULTS AND DISCUSSIONS

3.1. Wet-etch-reconditioning process development:

In contrast to bulk Ge, the nanostructured Ge is characterized by a large surface area, which induces a different reactivity compared to a bulk substrate. To shed light on the

polishing behavior of the different mixtures on nanostructured non-epi-ready Ge wafers, we first consider fresh PGe samples as test vehicles to determine a suitable composition mixture to recondition the detached wafers. To determine the most suitable composition for reconditioning purposes, three typical mixtures have been tested on PGe: (1) dilute Ammonia Peroxide Mixture (APM, $NH_4OH:H_2O_2:H_2O$, 1:1:5, v-v-v), (2) dilute Hydrochloric acid Peroxide Mixture (HPM, $HCl:H_2O_2:H_2O$, 1:1:7, v-v-v), and (3) HF-based solution ($HF:H_2O_2:H_2O$, 1:3:6, v-v-v). After APM and HPM etching, the surface exhibits a rough topography with the presence of either GeO_x-based crystals or residues, making these solutions unsuitable for reconditioning purposes (Fig. S2). Conversely, after HF-based solution etching, a defect-free surface is obtained after PGe etching. The rest of this study will focus on this type of mixture.

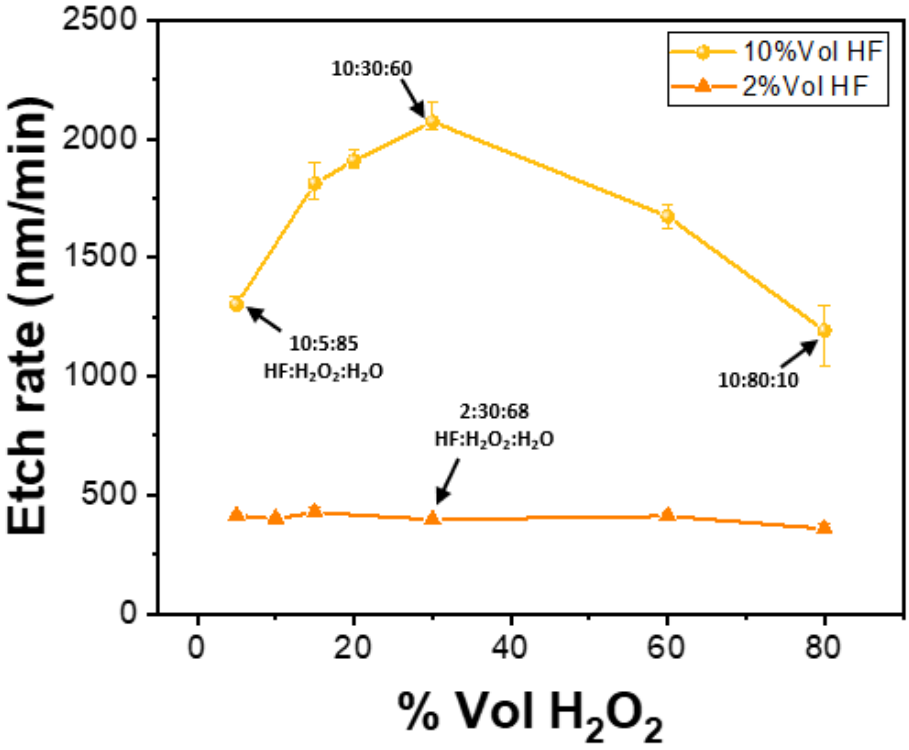

Fig. 2: Etch rate as a function of %Vol of H_2O_2 for 2%Vol HF (orange triangles) and 10%Vol HF (yellow dots) on Ge bulk material (room temperature, 600 RPM). For more details, four mixture compositions are indicated ($HF:H_2O_2:H_2O$, v-v-v).

The etching behavior of the HF-based solutions on nanostructured Ge has been further investigated to determine a solution suitable for our reconditioning process. Fig. 2 represents the etch rates obtained on bulk material for an HF volume percentage equal to 2% and 10% as a function of the volume percentage of H_2O_2, completed with water to keep both the HF concentration and the mixture's volume constant. From these measures, it is evident that when using solutions with 2%Vol of HF, the etch rates are relatively low (<500 nm/min) and not affected by the volume percentage of H_2O_2. Interestingly, for higher 10%Vol of HF, the etch rate is found to increase first with increasing the %Vol of H_2O_2, reaching a maximum of 30%Vol before decreasing monotonously. The increasing etch rate domain seems to be governed by an excess HF regime and the etching is then limited by the oxidation of the surface. Conversely, for a higher %Vol of H_2O_2, a uniformly oxidized surface can be formed and subsequently dissolved [39]. The etching of the oxidized Ge-based compounds becomes the rate-limiting step of the etching process. The decrease in the etching rate is likely due to the higher proportion of H_2O_2 in the stagnant film present on the surface of the substrate, which will induce a higher mass-transfer control of the HF etching at the surface of the Ge [40]. In addition, increasing the H_2O_2 concentration could also favor the formation of Ge-OH bonds instead of Ge-F formed when Ge surface atoms are in contact with HF. Due to the higher electronegativity difference between Ge and F than between Ge and O (2.0 Vs 1.4), the Ge-F bond is supposed to be more ionic than the Ge-O. This polarizing nature of Ge-F weakens the back bond and induces a Ge atom release [35]. The increase in Ge-OH quantity by increasing

the H_2O_2 proportion has a surface stabilization effect and reduces the etch rate at fixed %Vol of HF.

The nanostructured Ge etching can be separated into two etching steps: the nanostructure etching followed by the bulk material flattening. During the nanostructure etching, a substantial amount of Ge (hydro)suboxides can accumulate on the nanostructure surface. These suboxides can hamper the etching due to their limited solubility [33]. These deposits cause high surface roughness, as observed with a low %Vol of HF, and make this etching domain unsuitable for the substrate reconditioning process (Fig. S3). To avoid this anisotropic behavior, while maintaining the etching rates in the order of a few µm/min, the volume percentage of HF is then fixed at 10%Vol to increase the desorption/dissolution rate of these oxidized compounds [29,33,39].

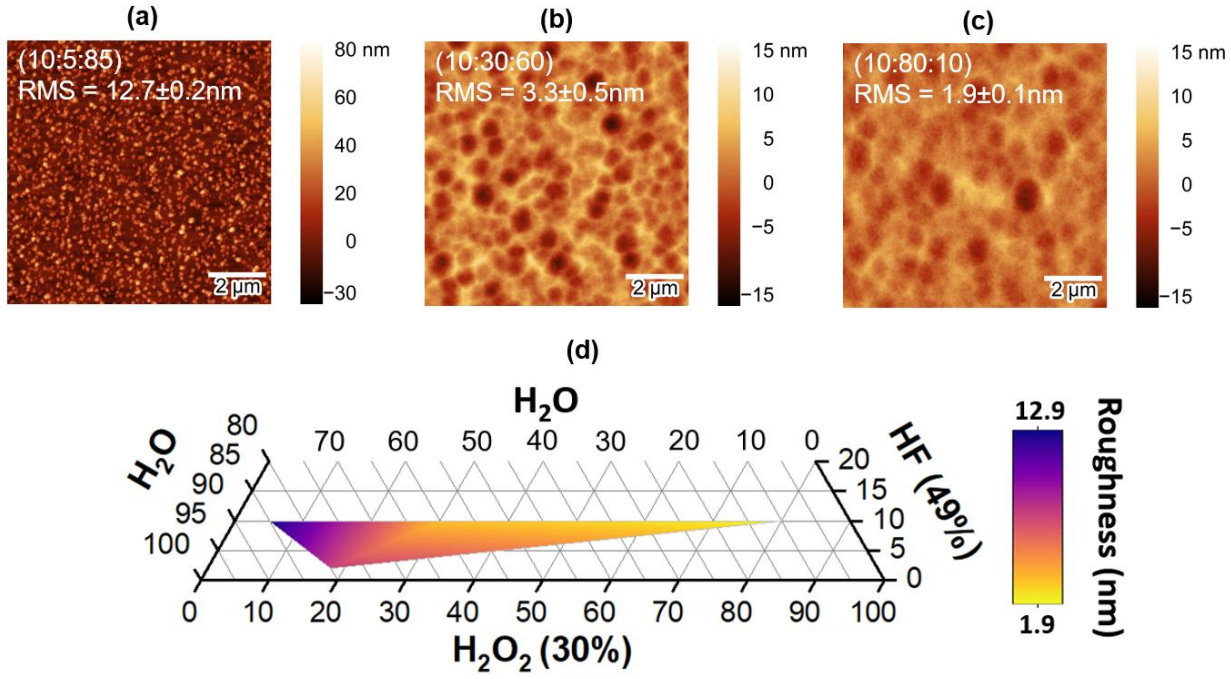

Fig. 3: AFM scans after PGe etching with different HF:H_2O_2:H_2O volumetric ratios: (a) 10:5:85 (b) 10:30:60 (c) 10:80:10 after 5 µm of etching. (d) Triphasic diagram of the roughness vs. reagent %Vol.

Fig. 3 (a-c) shows AFM scans and RMS roughness of PGe samples after wet etching with different HF:H_2O_2:H_2O volumetric ratios. These etched surfaces are obtained after only 5 µm of etching, i.e., 3 min 51 s, 2 min 59 s, and 4 min 12 s of etching, respectively (Fig. 2). With a lack of oxidizing agents (H_2O_2 < 30 %Vol, Fig. 3 (a)), the oxidation is non-uniform across the surface of the nanostructure, and a strong anisotropic etching is observed. As a result, a high roughness of 12.7 ± 0.2 nm (Fig. 3 (a) and Fig. S3) indicates that this etching domain is unsuitable for the reconditioning process. Conversely, when the oxide layer can form homogeneously (H_2O_2 > 30 %Vol, Fig. 3 (b-c)) on the entire surface area of the nanostructured PGe, all the surface structures are efficiently removed, and a flat surface with a roughness of 3.3 ± 0.5 nm is obtained using a 10:30:60 (HF:H_2O_2:H_2O) solution (Fig. 3 (b)).

The residual roughness of 3 nm is caused by the formation of pits on the surface due to the Ge nanostructuration during porosification (Fig. S4). By promoting a diffusion-limited etching by HF at the surface with a large excess of the oxidizing agent, it is possible to reduce this roughness during the bulk material flattening step, as shown on bulk Si [40,41] and recently on bulk Ge [9]. An activation energy of 11.3 kJ/mol (Fig. S5) for a 10:80:10 (HF:H_2O_2:H_2O) solution indicates a mixed dependence between kinetics and diffusion for the etching [33]. The rotation rate has been deliberately set at 600 RPM, allowing achieving a constant etch rate. The mixed control by HF diffusion allows reducing the roughness from 21.6 ± 0.1 nm before etching to 3.3 ± 0.5 nm (Fig. 3 (b)) to 2.5 ± 0.2 nm (Fig. S6), then 1.9 ± 0.1 nm (Fig. 3 (c)) after the etching in solutions with volumetric ratios of 10:30:60, 10:60:30, and 10:80:10, respectively. The triphasic diagram in Fig. 3 (d) summarizes the results obtained for the surface roughness.

To better describe and evaluate surface geometrical characteristics, shape distribution parameters skewness, kurtosis, and autocorrelation length are introduced (Fig. S7) [42]. The

surface after etching with the volumetric ratio 10:5:85 exhibits a large positive skewness value (1.19) meaning that this surface has round valleys and sharp peaks due to the residues left after etching. Conversely, the slight negative values exhibited after etching with the mixtures 10:30:60 and 10:80:10 (-0.6 and -0.4, respectively) show that these surfaces tend to have globally centered heights around the mean line with few sharp valleys and rounded peaks. In addition, the decreased value of kurtosis when the %Vol H_2O_2 is increased (4.0, 3.33, and 3.09 for 10:5:85, 10:60:10, and 10:80:10 mixture, respectively) indicates a lower degree of peakedness for the mixture with the highest %Vol of H_2O_2, which means a flatter surface with a height distribution close to a Gaussian distribution. Finally, the autocorrelation length increases with the %Vol of H_2O_2, confirmed by the increase of pit-like features' size seen on AFM scans (Fig. 3 (b-c)).

To conclude, increasing the volume percentage of H_2O_2, with fixed %Vol of HF, allows reducing the surface roughness after etching by reducing the number of peaks and/or valleys after etching and/or reducing their amplitude. The 10:80:10 volumetric ratio is suitable for the wet-etch-reconditioning application.

3.2. Chemical reconditioning of detached Ge substrates with various pillar sizes:

In our previous work, we demonstrated the feasibility of the PEELER process [26]. To extend the scope of our method and test its robustness to etch isotropically different nanostructures, the most suitable studied composition ($HF:H_2O_2:H_2O$, 10:80:10) is tested on detached substrates after NM separation with various pillar features. Fig. 4 (a) depicts the structure after epitaxy (as-grown structure). As an inset, the top-view SEM image after the NM detachment is illustrated. From the inset of Fig. 4 (a), the lift-off of the as-grown Ge epi-layer leaves broken pillars with a surface density around 45 μm^{-2} and a mean diameter of 37 nm (Fig. S8). To vary pillar size and density, post-growth thermal anneals are performed on two as-grown

samples for 1 h at 600 °C and for 1 h at 700 °C, respectively (Fig. 4 (b-c)). Post-growth thermal treatment is found to cause a morphological transformation of the separation layer by means of Ostwald Ripening phenomena [19,43,44]. This results in a reduced pillar density in favor of an increased mean diameter and a slight shrinkage of the separation layer's height from approximately 110 nm down to 105 nm. Accordingly, as shown by the plan view SEM observations of the three samples' surface morphology after NM's separation (insets in Fig. 4 (b-c)), pillars with a mean diameter around 44 nm and 110 nm are obtained after annealing for 1 h at 600 °C and at 700 °C (Fig. S8). The increased pillar size is accompanied by a reduction in their density from 45 μm^{-2} down to 0.7 μm^{-2} after the annealing at 700 °C for 1 h. The maximum pillar diameter is around 130 nm and 500 nm after annealing for 1 h at 600 °C and at 700 °C, respectively (Fig. S8). These pillar distributions allow assessing the effectiveness of the proposed solution for substrate chemical reconditioning and reuse.

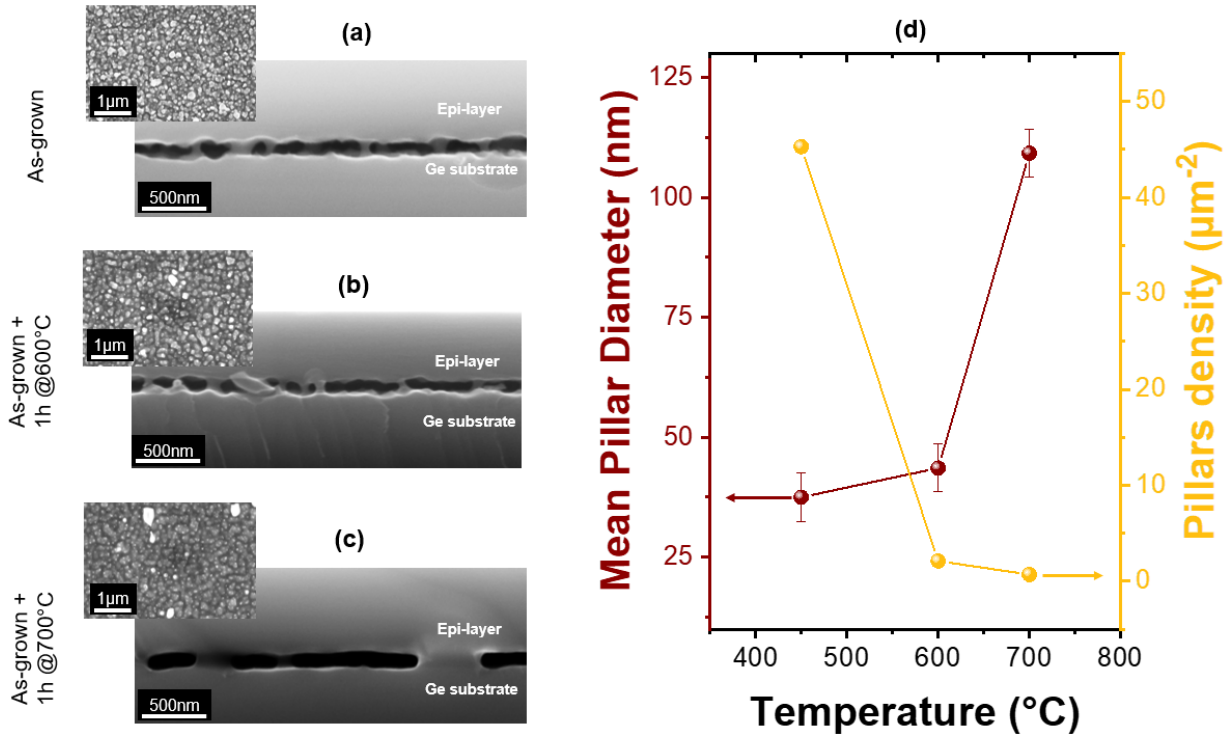

Fig. 4: SEM cross-sectional images illustrating the void-layer with the epi-layer and the Ge substrate with top-view SEM images of the substrate after NM detachment as an inset: (a) as-grown structure, (b) as-grown structure after 600 °C annealing for 1 h, and (c) as-grown structure after 700 °C annealing for 1 h. (d) Pillars' mean diameter and pillar density as a function of the annealing temperature.

After only 5 µm Ge etching per wafer's side, *i.e.*, 4 min and 12 s of total etching time (Fig. 2), the broken pillars are successfully removed, leaving pillar-free, flat surfaces on top of reconditioned substrates (Fig. 5 (d-e), Fig. S9). The surface roughness after chemical reconditioning (step (***iv***) in Fig. 1 (a)) is 2.4 ± 0.1 nm for the As-grown sample and 2.5 ± 0.2 nm for those annealed at 600 °C and 700 °C for 1 h (Fig. 5 (d), Fig. S10). This demonstrates that our reconditioning process enables smoothing of the surface down to ≤ 2.5 nm RMS for all surface morphologies obtained with various pillar sizes, including structures with a strong porous layer reorganization and the presence of large pillars with a diameter of up to 500 nm. The obtained values, in this work, are comparable to the reported reconditioned substrate's RMS of 3.1 nm for porous silicon [45], shown to be suitable to produce high-quality Si NM's for PV applications.

Additionally, the skewness, kurtosis, and autocorrelation length values have been determined for each initial condition after the wet-etch-reconditioning process (Fig. S7). Globally, the shape distribution parameters of each sample are close to each other, meaning a similar topography regardless of the initial annealing conditions. The slight negative skewness value demonstrates that surfaces tend to have their heights globally centered around the mean line, with few sharp valleys and rounded peaks. In addition, the kurtosis values slightly under 3 demonstrate a low level of peakedness. Finally, a slight increase in the autocorrelation length values exhibits a slight increase in pit-like feature size as the initial annealing temperature

increases. To conclude, regardless of the initial annealing conditions, the similar surface topography is obtained after pillar etching. These results confirm the robustness of the process and its potential application for macroporous approaches using µm-scale pillars (GON) [13,14] and direct III-V materials growth on double PGe layers [24,27], leaving pillars with hundreds of nanometers. Furthermore, our process showcases a sustainable and efficient approach with only 5 µm of etching per wafer's side within a relatively short duration, making it directly applicable in the industry.

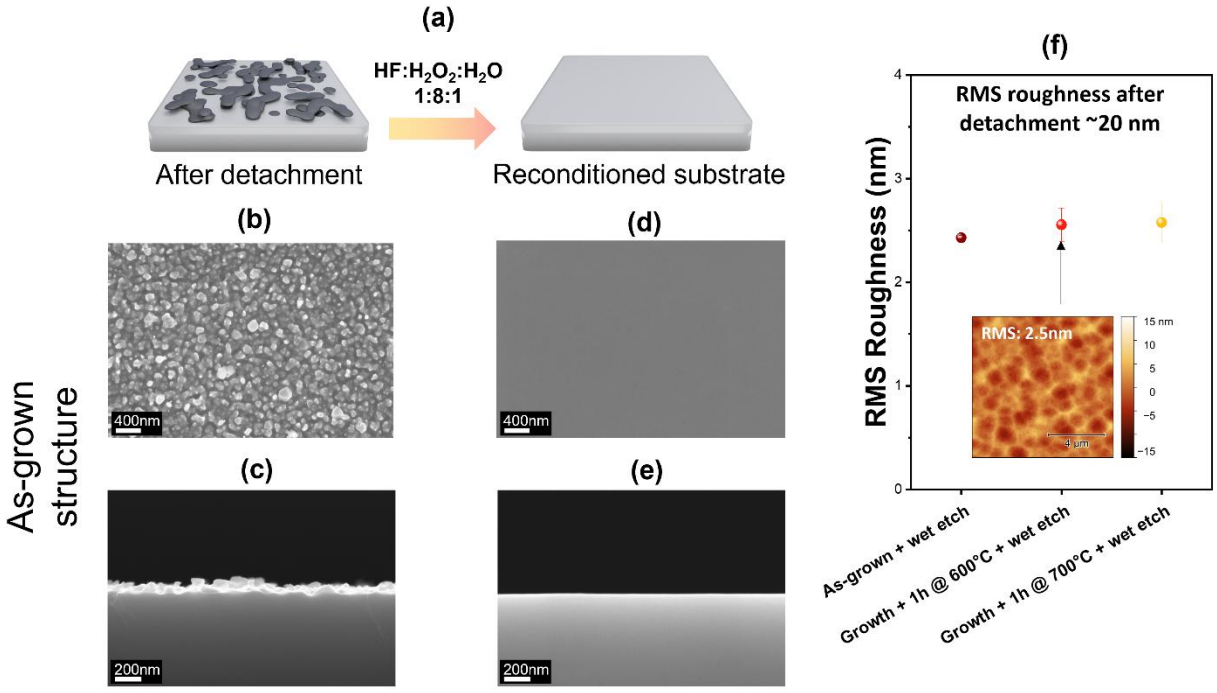

Fig. 5: (a) Reconditioning process flow applied to detached substrates. (b-c) SEM top-view and cross-sectional images of the As-grown structure after detachment. (d-e) SEM top-view and cross-sectional images of the As-grown structure after wet etching with HF:H_2O_2:H_2O (1:8:1, v-v-v). (f) RMS roughness after the reconditioning process of detached substrates for different annealing temperatures.

3.3. Porous layer formation on a reconditioned Ge surface:

As the targeted goal of the proposed approach is to obtain a porous layer on reconditioned substrates with identical structural characteristics (thickness, in-plane, and in-depth morphology, porosity) to the one obtained for the first PEELER cycle with a suitable surface topography for further epitaxial growth, the same porosification process is applied on both reconditioned and epi-ready substrates. Accordingly, the PGe layer obtained on epi-ready Ge substrate (PGe1, hereafter) is used as a reference and compared to the second PGe (PGe2, hereafter) layer produced on the same wafer after epitaxial layer lift-off and chemical reconditioning. Indeed, considering the employed porosification cell we recently developed [46] along with the BEE upscale method [21], allowing forming reproducible PGe layers with high spatial uniformity across large surfaces, the PGe quality and spatial uniformity of the second BEE run will mainly depend on the quality of the reconditioned substrate surface. Accordingly, Fig. 6 (a) shows the XRR spectrum recorded from the first and the second porosification cycles. We obtain the same PGe layer critical angle of 0.41 ° corresponding to an equal porosity around 52% for both PGe1 and PGe2 samples. As the XRR allows probing centimeter-scale surfaces, the preservation of the same porosity is a good indication of the overall PGe2 uniformity. This result is expected, since the reconditioning process provides a residue-free flat sample's surface (Fig. S9). Moreover, as demonstrated by the cross-sectional and plan view SEM observations (Fig. 6 (b-e)), the thickness, the in-depth, and in-plane morphologies of the PGe layers are also identical for both cycles. Finally, a morphological investigation by AFM revealed a surface roughness of PGe2 of 2.2 ± 0.2 nm (Fig. 6 (f-g)). This variation of PGe's surface roughness remains below 1 nm, and it is not expected to significantly alter the epitaxial structure properties [21,26]. These results demonstrate that the proposed chemical reconditioning approach can be successfully applied to Ge substrate reuse after the lift-off process. Furthermore, we expect a similar result on both p-

type (this work) and n-type substrates due to the chemical nature of the etching in H_2O_2-based mixture [29,33,34]. This indicates the validity of our reconditioning approach to obtain a porous layer ready for epitaxy on reconditioned substrate and allows its reuse for new epitaxial growth and further cycles as described in Fig. 1 (a).

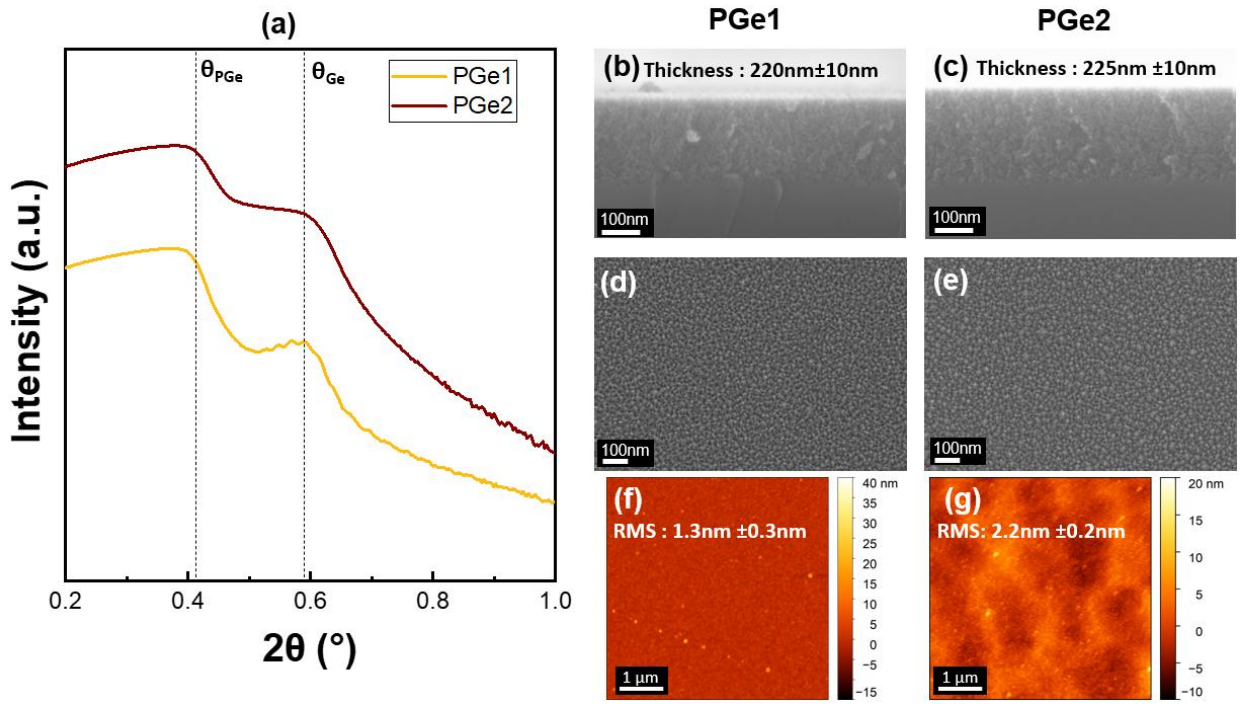

Fig. 6: (a) XRR spectra comparison between the porous layer on an epi-ready substrate (PGe1, reference) and the porous layer on a reconditioned substrate (PGe2, Reporosification), (b-c) cross-sectional SEM images (d-e) Top-view images and (f-g) AFM scans of the reference porous layer and the porous layer on a reconditioned substrate, respectively.

4. CONCLUSIONS

In this work, we investigate three different mixtures based on dilute ammonia peroxide mixtures, dilute hydrochloric acid peroxide mixtures, and HF-based solutions as a potential alternative to the costly CMP process for Ge substrate reconditioning after the porous lift-off process. HF:H_2O_2:H_2O mixtures exhibit a polishing behavior of nanostructured Ge, and an

experimental demonstration of substrate reuse has been established. With the investigation of the etching mechanisms involved in the polishing of nanostructured Ge surfaces, a solution with a volume ratio of (10:80:10) was determined to be suitable for substrate reconditioning. The robustness of our approach was tested on surfaces with pillar diameters ranging from 37 nm up to 500 nm obtained after post-growth thermal annealing at various temperatures. We succeeded in smoothing the detached Ge substrate by chemical etching and obtaining a low surface roughness (< 2.5 nm RMS) after only 5 µm of etching, regardless of the initial surface morphology, proving its compatibility with porous and other lift-off techniques. Using this reconditioning process, we obtained a porous layer ready for epitaxy with characteristics identical to those obtained on epi-ready substrates (thickness, morphology, and porosity) and a low surface RMS roughness of 2.2 ± 0.2 nm.

The results demonstrated in this work allow us to unravel the wet etching mechanism of Ge nanostructures and make recommendations on the mix composition for reconditioning mixture development. Additionally, in contrast with our previous proof-of-concept, the present study broadens the range of potential applications for our wet approach by incorporating various nano- and micro-sized porous structures. Our wet approach offers a cost-efficient alternative to expensive CMP polishing tools. Our method is fast and easily applicable on an industrial scale, with only 4 min of etching, and allows minimal Ge consumption during each cycle with only 5 µm/side etched during the wet-etch-reconditioning process. This method has the potential to significantly reduce the cost associated with the manufacturing of optoelectronic devices using various thin-film release methods.

5. ACKNOWLEDGMENTS

The authors thank and the 3IT's clean room staff for technical support. The authors also thank the Natural Sciences and Engineering Research Council of Canada (NSERC), Innovation en énergie électrique (InnovÉÉ), Mitacs, Umicore and Saint-Augustin Canada Electric (Stace) for financial support. A special mention is addressed to Nicolas Paupy and Jonathan Henriques, for their valuable assistance. LN2 is a joint International Research Laboratory (IRL 3463) funded and co-operated in Canada by Université de Sherbrooke and in France by CNRS as well as ECL, INSA Lyon, and Université Grenoble Alpes (UGA). It is also supported by the Fonds de Recherche du Québec Nature et Technologie (FRQNT).

6. CREDIT AUTHOR STATEMENT:

The manuscript was written through the contributions of all authors. All authors have given approval to the final version of the manuscript. **A. Chapotot.:** Conceptualization, Methodology, Formal analysis, Investigation, Writing-Original Draft, Writing – Review & Editing, Visualization. **B. Ilahi.:** Conceptualization, Methodology, Writing-Original Draft, Writing – Review & Editing, Supervision. **J. Arias-Zapata.:** Review & Editing, Supervision. **T. Hanuš.:** Review & Editing, Investigation. **A. Ayari.:** Review & Editing, Investigation. **G. Hamon.:** Review & Editing, Supervision. **J.Cho.:** Review & Editing. **K.Dessein.:** Review & Editing. **M. Darnon.:** Supervision, Funding acquisition, Review & Editing. **A. Boucherif:** Conceptualization, Supervision, Funding acquisition, Review & Editing.

7. REFERENCES

[1] S.P. Adiga, C. Jin, L.A. Curtiss, N.A. Monteiro-Riviere, R.J. Narayan, Nanoporous membranes for medical and biological applications: Nanoporous membranes for medical and biological applications, WIREs Nanomed Nanobiotechnol. 1 (2009) 568–581. https://doi.org/10.1002/wnan.50.

[2] A. Dupuy, A. Roland, M.R. Aziziyan, S. Sauze, D. Machon, R. Arès, A. Boucherif, Monolithic integration of mesoporous germanium: A step toward high-performance on-chip

anode, Materials Today Communications. 26 (2021) 101820. https://doi.org/10.1016/j.mtcomm.2020.101820.
[3] Best Research-Cell Efficiency Chart, (n.d.). https://www.nrel.gov/pv/cell-efficiency.html (accessed January 20, 2023).
[4] R.R. King, D.C. Law, K.M. Edmondson, C.M. Fetzer, G.S. Kinsey, H. Yoon, R.A. Sherif, N.H. Karam, 40% efficient metamorphic GaInP/GaInAs/Ge multijunction solar cells, Appl. Phys. Lett. 90 (2007) 183516. https://doi.org/10.1063/1.2734507.
[5] G.M. Wilson, M. Al-Jassim, W.K. Metzger, S.W. Glunz, P. Verlinden, G. Xiong, L.M. Mansfield, B.J. Stanbery, K. Zhu, Y. Yan, J.J. Berry, A.J. Ptak, F. Dimroth, B.M. Kayes, A.C. Tamboli, R. Peibst, K. Catchpole, M.O. Reese, C.S. Klinga, P. Denholm, M. Morjaria, M.G. Deceglie, J.M. Freeman, M.A. Mikofski, D.C. Jordan, G. TamizhMani, D.B. Sulas-Kern, The 2020 photovoltaic technologies roadmap, J. Phys. D: Appl. Phys. 53 (2020) 493001. https://doi.org/10.1088/1361-6463/ab9c6a.
[6] K.A. Horowitz, T.W. Remo, B. Smith, A.J. Ptak, A Techno-Economic Analysis and Cost Reduction Roadmap for III-V Solar Cells, 2018. https://doi.org/10.2172/1484349.
[7] J.S. Ward, T. Remo, K. Horowitz, M. Woodhouse, B. Sopori, K. VanSant, P. Basore, Techno-economic analysis of three different substrate removal and reuse strategies for III-V solar cells: Techno-economic analysis for III-V solar cells, Prog. Photovolt: Res. Appl. 24 (2016) 1284–1292. https://doi.org/10.1002/pip.2776.
[8] I. Lombardero, M. Ochoa, N. Miyashita, Y. Okada, C. Algora, Theoretical and experimental assessment of thinned germanium substrates for III–V multijunction solar cells, Prog Photovolt Res Appl. 28 (2020) 1097–1106. https://doi.org/10.1002/pip.3281.
[9] C. Sanchez-Perez, I. Garcia, I. Rey-Stolle, Fast chemical thinning of germanium wafers for optoelectronic applications, Applied Surface Science. 579 (2022) 152199. https://doi.org/10.1016/j.apsusc.2021.152199.
[10] G. Van Hoof, M. Schurmans, B. Robertz, J.-F. Ménard, K. Dessein, Moving Towards Sustainable Germanium Sourcing Evaluated by Means of Life Cycle Assessment, J. Sustain. Metall. 6 (2020) 333–343. https://doi.org/10.1007/s40831-020-00277-4.
[11] N. Pan, Epitaxial lift-off of large-area GaAs multi-junction solar cells for high efficiency clean and portable energy power generation, in: 2014 IEEE International Conference on Semiconductor Electronics (ICSE2014), 2014: pp. 347–349. https://doi.org/10.1109/SMELEC.2014.6920869.
[12] D. Shahrjerdi, S.W. Bedell, C. Ebert, C. Bayram, B. Hekmatshoar, K. Fogel, P. Lauro, M. Gaynes, T. Gokmen, J.A. Ott, D.K. Sadana, High-efficiency thin-film InGaP/InGaAs/Ge tandem solar cells enabled by controlled spalling technology, Appl. Phys. Lett. 100 (2012) 053901. https://doi.org/10.1063/1.3681397.
[13] S. Park, J. Simon, K.L. Schulte, A.J. Ptak, J.-S. Wi, D.L. Young, J. Oh, Germanium-on-Nothing for Epitaxial Liftoff of GaAs Solar Cells, Joule. 3 (2019) 1782–1793. https://doi.org/10.1016/j.joule.2019.05.013.
[14] V. Depauw, C. Porret, M. Moelants, E. Vecchio, K. Kennes, H. Han, R. Loo, J. Cho, G. Courtois, R. Kurstjens, K. Dessein, V. Orejuela, C. Sanchez- Perez, I. Rey- Stolle, I. García, Wafer- scale Ge epitaxial foils grown at high growth rates and released from porous substrates for triple- junction solar cells, Progress in Photovoltaics. (2022) pip.3634. https://doi.org/10.1002/pip.3634.
[15] B. Aspar, M. Bruel, H. Moriceau, C. Maleville, T. Poumeyrol, A.M. Papon, Basic mechanisms involved in the Smart-Cut* process, Microelectronic Engineering. (1997).

[16] T.M. Diallo, M.R. Aziziyan, R. Arvinte, J. Harmand, G. Patriarche, C. Renard, S. Fafard, R. Arès, A. Boucherif, In- Situ Transmission Electron Microscopy Observation of Germanium Growth on Freestanding Graphene: Unfolding Mechanism of 3D Crystal Growth During Van der Waals Epitaxy, Small. 18 (2022) 2101890. https://doi.org/10.1002/smll.202101890.
[17] H. Kim, S. Lee, J. Shin, M. Zhu, M. Akl, K. Lu, N.M. Han, Y. Baek, C.S. Chang, J.M. Suh, K.S. Kim, B.-I. Park, Y. Zhang, C. Choi, H. Shin, H. Yu, Y. Meng, S.-I. Kim, S. Seo, K. Lee, H.S. Kum, J.-H. Lee, J.-H. Ahn, S.-H. Bae, J. Hwang, Y. Shi, J. Kim, Graphene nanopattern as a universal epitaxy platform for single-crystal membrane production and defect reduction, Nat. Nanotechnol. 17 (2022) 1054–1059. https://doi.org/10.1038/s41565-022-01200-6.
[18] R.B. Bergmann, T.J. Rinke, R.M. Hausner, M. Grauvogl, M. Vetter, J.H. Werner, Thin film solar cells on glass by transfer of monocrystalline Si films, International Journal of Photoenergy. 1 (1999) 89–93. https://doi.org/10.1155/S1110662X99000173.
[19] A. Boucherif, G. Beaudin, V. Aimez, R. Arès, Mesoporous germanium morphology transformation for lift-off process and substrate re-use, Appl. Phys. Lett. 102 (2013) 011915. https://doi.org/10.1063/1.4775357.
[20] Y.A. Bioud, A. Boucherif, A. Belarouci, E. Paradis, S. Fafard, V. Aimez, D. Drouin, R. Arès, Fast growth synthesis of mesoporous germanium films by high frequency bipolar electrochemical etching, Electrochimica Acta. 232 (2017) 422–430. https://doi.org/10.1016/j.electacta.2017.02.115.
[21] T. Hanuš, J. Arias- Zapata, B. Ilahi, P. Provost, J. Cho, K. Dessein, A. Boucherif, Large- Scale Formation of Uniform Porous Ge Nanostructures with Tunable Physical Properties, Adv Materials Inter. (2023) 2202495. https://doi.org/10.1002/admi.202202495.
[22] A. Dupuy, M.R. Aziziyan, D. Machon, R. Arès, A. Boucherif, Anisotropic mesoporous germanium nanostructures by fast bipolar electrochemical etching, Electrochimica Acta. 378 (2021) 137935. https://doi.org/10.1016/j.electacta.2021.137935.
[23] E. Garralaga Rojas, B. Terheiden, H. Plagwitz, J. Hensen, C. Baur, G.F.X. Strobl, R. Brendel, Formation of mesoporous germanium double layers by electrochemical etching for layer transfer processes, Electrochemistry Communications. 12 (2010) 231–233. https://doi.org/10.1016/j.elecom.2009.11.033.
[24] E. Winter, W. Schreiber, P. Schygulla, P.L. Souza, S. Janz, D. Lackner, J. Ohlmann, III-V Material Growth on Electrochemically Porosified Ge Substrates, Journal of Crystal Growth. (2022) 126980. https://doi.org/10.1016/j.jcrysgro.2022.126980.
[25] T. Hanuš, B. Ilahi, A. Chapotot, H. Pelletier, J. Cho, K. Dessein, A. Boucherif, Wafer-scale Ge freestanding membranes for lightweight and flexible optoelectronics, Materials Today Advances. 18 (2023) 100373. https://doi.org/10.1016/j.mtadv.2023.100373.
[26] N. Paupy, Z. Oulad Elhmaidi, A. Chapotot, T. Hanuš, J. Arias-Zapata, B. Ilahi, A. Heintz, A.B. Poungoué Mbeunmi, R. Arvinte, M.R. Aziziyan, V. Daniel, G. Hamon, J. Chrétien, F. Zouaghi, A. Ayari, L. Mouchel, J. Henriques, L. Demoulin, T.M. Diallo, P.-O. Provost, H. Pelletier, M. Volatier, R. Kurstjens, J. Cho, G. Courtois, K. Dessein, S. Arcand, C. Dubuc, A. Jaouad, N. Quaegebeur, R. Gosselin, D. Machon, R. Arès, M. Darnon, A. Boucherif, Wafer-scale detachable monocrystalline germanium nanomembranes for the growth of III–V materials and substrate reuse, Nanoscale Adv. (2023) 10.1039.D3NA00053B. https://doi.org/10.1039/D3NA00053B.

[27] A. Cavalli, N. Alkurd, S. Johnston, D.R. Diercks, D.M. Roberts, B.E. Ley, J. Simon, D.L. Young, C.E. Packard, A.J. Ptak, Performance of III–V Solar Cells Grown on Reformed Mesoporous Ge Templates, IEEE J. Photovoltaics. (2021) 1–7. https://doi.org/10.1109/JPHOTOV.2021.3120514.
[28] V. Steckenreiter, J. Hensen, A. Knorr, S. Kajari-Schroder, R. Brendel, Reuse of Substrate Wafers for the Porous Silicon Layer Transfer, IEEE J. Photovoltaics. 6 (2016) 783–790. https://doi.org/10.1109/JPHOTOV.2016.2545406.
[29] I.M. Huygens, W.P. Gomes, K. Strubbe, Etching of Germanium in Hydrogenperoxide Solutions, ECS Trans. 6 (2007) 375–386. https://doi.org/10.1149/1.2731205.
[30] N.N. Golovnev, V.B. Nogteva, I.I. Golovneva, Formation of Si(IV) and Ge(IV) Fluoride Complexes in Dilute Aqueous Solutions, Russian Journal of General Chemistry. 73 (2003) 1388–1394. https://doi.org/10.1023/B:RUGC.0000015984.57174.57.
[31] S. Sioncke, D.P. Brunco, M. Meuris, O. Uwamahoro, J. Van Steenbergen, E. Vrancken, M.M. Heyns, Etch Rate Study of Germanium, GaAs and InGaAs: A Challenge in Semiconductor Processing, SSP. 145–146 (2009) 203–206. https://doi.org/10.4028/www.scientific.net/SSP.145-146.203.
[32] D.R. Turner, On the Mechanism of Chemically Etching Germanium and Silicon, J. Electrochem. Soc. 107 (1960) 810. https://doi.org/10.1149/1.2427519.
[33] G.H.A. Abrenica, M. Fingerle, M.V. Lebedev, S. Arnauts, T. Mayer, F. Holsteyns, S. de Gendt, D.H. van Dorp, Wet Chemical Processing of Ge in Acidic H_2O_2 Solution: Nanoscale Etching and Surface Chemistry, ECS J. Solid State Sci. Technol. 9 (2020) 084002. https://doi.org/10.1149/2162-8777/abb1c5.
[34] H. Gerischer, W. Mindt, The mechanisms of the decomposition of semiconductors by electrochemical oxidation and reduction, Electrochimica Acta. 13 (1968) 1329–1341. https://doi.org/10.1016/0013-4686(68)80060-X.
[35] P. Ponath, A.B. Posadas, A.A. Demkov, Ge(001) surface cleaning methods for device integration, Applied Physics Reviews. 4 (2017) 021308. https://doi.org/10.1063/1.4984975.
[36] H. Sivaramakrishnan Radhakrishnan, R. Martini, V. Depauw, K. Van Nieuwenhuysen, T. Bearda, I. Gordon, J. Szlufcik, J. Poortmans, Kerfless layer-transfer of thin epitaxial silicon foils using novel multiple layer porous silicon stacks with near 100% detachment yield and large minority carrier diffusion lengths, Solar Energy Materials and Solar Cells. 135 (2015) 113–123. https://doi.org/10.1016/j.solmat.2014.10.049.
[37] F. Zouaghi, A. Ayari, B. Ilahi, J. Chretien, T. Hanus, N. Paupy, N. Quaegebeur, A. Boucherif, Impact of Thermal Annealing on the Mechanical Properties of Ge epilayer on Mesoporous Germanium for Layer Separation and Substrate Re-use, in: 2022 IEEE 49th Photovoltaics Specialists Conference (PVSC), IEEE, Philadelphia, PA, USA, 2022: pp. 627–627. https://doi.org/10.1109/PVSC48317.2022.9938456.
[38] S.A. Veldhuis, P. Brinks, T.M. Stawski, O.F. Göbel, J.E. ten Elshof, A facile method for the density determination of ceramic thin films using X-ray reflectivity, J Sol-Gel Sci Technol. (2014). https://doi.org/10.1007/s10971-014-3336-2.
[39] S. Kagawa, T. Mikawa, T. Kaneda, Chemical Etching of Germanium with H_3PO_4–H_2O_2–H_2O Solution, Jpn. J. Appl. Phys. 21 (1982) 1616–1618. https://doi.org/10.1143/JJAP.21.1616.
[40] M.S. Kulkarni, A Review and Unifying Analysis of Defect Decoration and Surface Polishing by Chemical Etching in Silicon Processing, Ind. Eng. Chem. Res. 42 (2003) 2558–2588. https://doi.org/10.1021/ie020716y.

[41] B. Tuck, The chemical polishing of semiconductors, J Mater Sci. 10 (1975) 321–339. https://doi.org/10.1007/BF00540357.
[42] E.S. Gadelmawla, M.M. Koura, T.M.A. Maksoud, I.M. Elewa, H.H. Soliman, Roughness parameters, Journal of Materials Processing Technology. 123 (2002) 133–145. https://doi.org/10.1016/S0924-0136(02)00060-2.
[43] S. Tutashkonko, T. Nychyporuk, V. Lysenko, M. Lemiti, Thermally induced Ostwald ripening of mesoporous Ge nanostructures, Journal of Applied Physics. 113 (2013) 023517. https://doi.org/10.1063/1.4775576.
[44] M.N. Beattie, Y.A. Bioud, D.G. Hobson, A. Boucherif, C.E. Valdivia, D. Drouin, R. Arès, K. Hinzer, Tunable conductivity in mesoporous germanium, Nanotechnology. 29 (2018) 215701. https://doi.org/10.1088/1361-6528/aab3f7.
[45] A. Hajijafarassar, K. Van Nieuwenhuysen, I. Sharlandzhiev, V. Depauw, H. Sivaramakrishnan Radhakrishnan, T. Bearda, M. Debucquoy, I. Gordon, J. Szlufcik, Y. Abdulraheem, J. Poortmans, L. Magagnin, Multiple Reuse of the Silicon Substrate in a Porous Silicon Based Layer Transfer Process, 32nd European Photovoltaic Solar Energy Conference and Exhibition; 313-316. (2016) 4 pages, 6251 kb. https://doi.org/10.4229/EUPVSEC20162016-2BO.2.6.
[46] Philippe-Olivier Provost, Abderraouf Boucherif, Wafer Receiver, electrochemical porosification apparatus and method using same, US 63/248,594. 2021. ⟨hal-03683618⟩, n.d.